First-principles studies of the electronic properties of native and substitutional anionic defects in bulk iron pyrite

Jun Hu,[1] Yanning Zhang,[1] Matt Law,[2] and Ruqian Wu[1,*]

[1]*Department of Physics and Astronomy, University of California, Irvine, California 92697-4575, USA*

[2]*Department of Chemistry and Department of Chemical Engineering and Materials Science, University of California, Irvine, California 92697, USA*

(Received 28 October 2011; revised manuscript received 22 December 2011; published 13 February 2012)

Systematic spin-polarized density functional theory calculations were performed to investigate the formation energies of native and substitutional anionic point defects in iron pyrite (FeS_2) and their impact on bulk electronic structure. A detailed analysis indicates that neutral sulfur and iron vacancies do not act as efficient donors or acceptors. We find that substitutional oxygen does not induce gap states in pyrite and can actually passivate gap states created by sulfur vacancies. Most Group V and VII impurities create mid-gap states and produce spin polarization. In particular, Cl and Br are shallow donors that introduce delocalized spin-polarized electrons for potential use in photovoltaic and spintronics applications.

DOI: 10.1103/PhysRevB.85.085203 PACS number(s): 71.55.−i, 72.40.+w, 61.72.Bb, 75.50.Pp

I. INTRODUCTION

The development of highly photoactive earth-abundant materials is critically urgent for both fundamental science and technological applications.[1,2] Iron pyrite (FeS_2) is a promising photovoltaic material because of its suitable band gap ($E_g = 0.95$ eV), strong light absorption ($\alpha > 10^5$ cm^{-1} for $h\nu > 1.4$ eV), long minority carrier diffusion length (100–1000 nm), and essentially infinite elemental abundance.[3–8] Pyrite photoelectrochemical and solid-state Schottky solar cells have shown large short-circuit current densities (30–42 mA cm^{-2}) and quantum efficiencies as high as 90%.[9,10] The main obstacle for the development of pyrite is its low open-circuit photovoltage (V_{OC}), which is typically only <200 mV.[8] Since 1984, a few dozen studies have explored possible causes of the low V_{OC}, such as bulk nonstoichiometry (mostly S or Fe vacancies),[8,11–13] surface states that cause Fermi pinning, thermionic-field emission, and large dark currents,[14–16] metallic FeS-like surface layers,[17,18] and small-band gap-phase impurities in the pyrite bulk (including marcasite, pyrrhotite, and amorphous iron sulfide phases).[9,19] Nevertheless, there still is no consensus as to the cause of the low V_{OC} or even the nature of the alleged gap states. The role of different point defects on the electronic and optical properties of bulk pyrite has not been systematically studied either experimentally or theoretically.

Equally important is to control the type, concentration, mobility, and diffusion length of charge carriers in pyrite by minimizing electronically active defects to enable rational doping. Experimental studies have demonstrated some degree of control in producing *n*-type pyrite samples by doping various elements. However, their transport properties such as carrier concentration, Hall mobility, and resistivity exhibit large variations depending on the fabrication methods.[20–27] On the other hand, although *p*-type doping with P or As has been reported, the source of hole carriers is ambiguous due to the weak dependence of transport properties on the concentration of impurities, rather small Hall voltage, and large uncertainty caused by poor contacts.[21,22,24] A clear understanding of the key factors that govern the transport properties of pyrite is indispensable for solar energy conversion applications. In particular, quantifying the ionization energies of the major impurities in pyrite would provide important guidance for experimental efforts.

Another possible use for pyrite is as a dilute magnetic semiconductor for spintronics applications.[28–30] Various semiconductors such as GaAs, ZnO, TiO_2, and GaN have been extensively studied, but their reported high-temperature ferromagnetism is now believed to be extrinsic, resulting mainly from precipitation of magnetic nanoparticles.[31] Incorporation of Co into pyrite at a concentration greater than 1% results in ferromagnetic ordering.[32,33] The narrow band gap and high carrier concentration of pyrite may permit a stronger exchange interaction among local magnetic moments and hence a higher Curie temperature.[34] Furthermore, Fe is known for its stable high-spin state in most environments, and its magnetization may be restored in pyrite by point defects such as vacancies or substitutional impurities. This may avoid the precipitation problem inherent in most dilute magnetic semiconductors that use 3d magnetic dopants as sources of spin polarization. Thus far, studies of magnetism in pyrite have received very little attention, and fundamental work in this direction should be very rewarding.

Here we report the results of systematic first-principles calculations to investigate the effects of neutral sulfur and iron-point defects and various neutral Group V and VII impurities on the electronic, optical, and magnetic properties of bulk pyrite. We find that both sulfur and iron vacancies (V_S and V_{Fe}) have large formation enthalpies and induce localized defect states with high ionization energies (>0.3 eV), such that these native defects are incapable of providing significant free carrier densities in pyrite. Oxygen substitution on sulfur sites (O_S) has a relatively small formation energy in oxidizing conditions but does not induce gap states in bulk pyrite, making O_S useful for passivating gap states induced by sulfur vacancies produced in sulfur-lean growth or annealing environments. Group V and VII dopants produce spin polarization in pyrite with a magnetic moment of 1.0 μ_B per impurity atom. While most of the Group V and VII dopants induce only deep defect levels, Cl_S and Br_S produce shallow donor or resonance levels that may be useful for photovoltaic and spintronic applications.

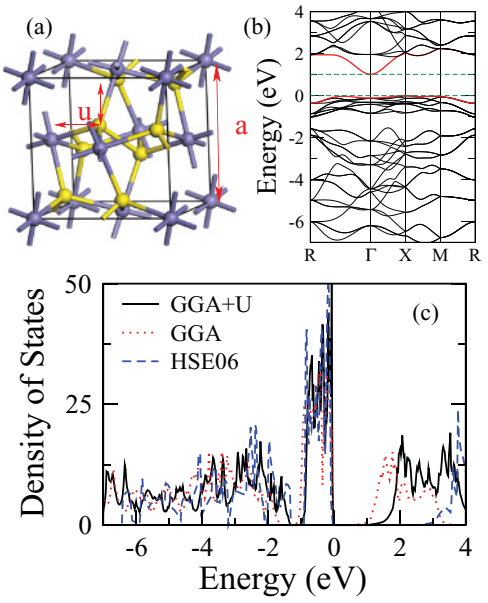

FIG. 1. (Color online) (a) The bulk unit cell of pyrite FeS_2. Violet (dark) and yellow (light) gray spheres represent Fe and S atoms, respectively. The parameters a and u denote the lattice constant and the distance between the S atom and the walls of the cubic box as indicated by the red arrows. (b) Band structure and (c) density of states (in states/eV·cell) of perfect pyrite. The valence band maximum (VBM) has been set as reference energy. The red/dark gray curves in (b) indicate the topmost valence band and lowest conduction band, and the horizontal green dashed lines indicate the VBM and conduction band minimum (CBM).

II. METHODS AND COMPUTATIONAL DETAILS

Spin-polarized density functional calculations were carried out with the Vienna *ab initio* simulation package (VASP)[35,36] at the level of the generalized gradient approximation (GGA) using the Perdew-Burke-Ernzerhof (PBE) functional.[37] We used the projector augmented wave (PAW) method for the description of the core-valence interaction.[38,39] The energy cutoff for the basis expansion was set to 350 eV. As sketched in Fig. 1(a), the pyrite FeS_2 structure belongs to the $Pa\bar{3}$ space group[40] and adopts a NaCl-like structure, with a face-centered cubic sublattice of diamagnetic Fe^{2+} ions and ⟨111⟩-oriented S-S dimers occupying the anion positions. Each Fe ion has an octahedral coordination to six S ions, and each S ion has three Fe neighbors and one S neighbor. The unit cell of the pyrite structure can be specified by two lattice parameters: the lattice constant a and the internal coordinate of S from the face of the unit cell u, as indicated in Fig. 1(a). To model individual point defects in pyrite, we used both $2 \times 2 \times 2$ supercells with 96 atoms and $3 \times 3 \times 3$ supercells with 324 atoms. A $7 \times 7 \times 7$ k-grid mesh was used to sample the Brillouin zone.[41] All atoms were fully relaxed until the calculated force on each atom was smaller than 0.01 eV/Å.

III. RESULTS AND DISCUSSION

A. Structural and electronic properties of bulk iron pyrite

As a benchmark test for our approach and parameterization, we first investigate the structural and electronic properties of perfect bulk pyrite. Regular GGA-PBE calculations usually underestimate the lattice constant and band gap of pyrite crystals; some previous calculations even predicted a metallic rather than a semiconducting state for bulk pyrite.[42,43] More sophisticated schemes such as the hybridized exchange-correlation functional (HSE06)[44] or Hubbard U correction[45] are therefore needed for reliable studies of pyrite systems. In this work we examined both HSE06 and GGA+U schemes and found that the latter, with $U = 2$ eV for Fe d-orbitals, is more appropriate for the correct description of electronic properties of bulk pyrite.

Our GGA+U calculations yield a nonmagnetic ground state for the bulk pyrite crystal, in agreement with experiment[46] and previous density functional theory (DFT) calculations.[19,47,48] As listed in Table I, the optimized lattice parameters, $a = 5.422$ Å and $u = 0.385$, are very close to the experimental values, $a = 5.418$ Å and $u = 0.385$.[49,50] An indirect band gap of 1.02 eV was obtained for bulk pyrite, as shown in Figs. 1(b) and 1(c). Similar results were reported recently by Sun *et al.* ($a = 5.424$ Å and $E_g = 1.03$ eV).[47] Experimental estimates of the pyrite band gap vary from 0.73 to 1.2 eV, with ∼0.95 eV the most widely accepted value.[3,51–56] From curves of density of states (DOS) in Fig. 1(c), one can see that regular GGA calculation underestimates the band gap by 0.52 eV, whereas the HSE06 calculation overestimates the gap by 1.67 eV relative to the GGA+U result. This situation was also reported in the previous literature.[19,47] The band structure in Fig. 1(b) shows that the valence band maximum (VBM) is close to the X-point and the conduction band minimum (CBM) is at the Γ-point of the Brillouin zone. We calculated an isotropic electron effective mass of $0.49m_e$ (m_e is the rest mass of a free electron) at the CBM. This agrees with the experimental value ($0.45m_e$)[49,53] but is larger than previous theoretical results, 0.35–$0.37m_e$.[57,58] The effective mass of holes at the VBM is anisotropic and ranges from $1.23m_e$ to $1.98m_e$, comparable to the experimental estimates, $2.2 \pm 0.7m_e$.[4] Using these effective masses, we obtained an intrinsic carrier density n_i of 2.7–3.8×10^{12} cm^{-3} at room temperature (300 K), with effective electron and hole densities of states $N_C = 2(2\pi m_e^* k_B T/h^2)^{3/2} = 8.6 \times 10^{18}$ cm^{-3} and $N_V =$

TABLE I. Properties of pyrite FeS_2: lattice constant a (Å), band gap E_g (eV), electron and hole effective masses m_e^* and m_h^* (m_e), intrinsic carrier density n_i ($\times 10^{12}$ cm^{-3}), and effective electron and hole densities of states N_C and N_V ($\times 10^{19}$ cm^{-3}). Values of n_i, N_C, and N_V are estimated at 300 K.

	a	E_g	m_e^*	m_h^*	n_i	N_C	N_V
The.	5.42	1.02	0.49	1.23 − 1.98	2.7 – 3.8	0.9	3.4 − 7.0
Exp.	5.42[49,50]	0.73 – 1.2[3,51,53,55]	0.45[49,53]	2.2 ± 0.7[4]	2.8[4]	0.3[4]	8.5 ± 5[4]

$2(2\pi m_h^* k_B T/h^2)^{3/2} = 3.4\text{–}7.0 \times 10^{19}$ cm^{-3}, again close to experimental values.[4] Wave function analysis reveals that the S-S $pp\sigma$, $pp\pi$, and $pp\pi^*$ bands have energies below -1.5 eV; the valence states between -1.0 eV and 0.0 eV have mostly the Fe 3d-t_{2g} character, and the conduction states between 1.02 eV and 4.2 eV are composed primarily of Fe-e_g and S-$pp\sigma^*$ orbitals.

Following the Bader charge division scheme,[59] we calculated the number of electrons on each atom in bulk pyrite, which results in charge states of Fe and S atoms of $+0.86e$ and $-0.43e$, respectively. We will use these values as references in the following discussions regarding the charge redistribution induced by native and nonnative defects. Note that these values are smaller in magnitude than the conventional oxidation states of pyrite defined in inorganic chemistry (Fe^{2+} and S^{1-}), due to the spatial division and the partial covalent feature of the Fe-S bonds. These values are somewhat smaller than the charges obtained using the Mulliken scheme ($+1.2e$ and $-0.6e$).[43]

B. Sulfur and iron vacancies

We considered various native defects in a $3 \times 3 \times 3$ supercell: including single sulfur vacancy (V_S), single iron vacancy (V_{Fe}), interstitial sulfur (S_i), sulfur-sulfur divacancy ($V_{S\text{-}S}$), and sulfur-iron divacancy ($V_{Fe\text{-}S}$). To quantitatively describe their energetics, we calculated formation energies according to

$$\Delta H_f = E(D) - E(FeS_2) + \Sigma n_D \mu_D. \quad (1)$$

Here $E(D)$ and $E(FeS_2)$ are total energies of the pyrite supercell with and without defects, respectively. μ_D and n_D represent the chemical potential and number of sulfur or iron atoms that are removed or added. To allow direct comparison between iron and sulfur defects, we also assumed an equilibrium growth/annealing condition with a constraint

$$2\Delta\mu_S + \Delta\mu_{Fe} = \Delta\mu_{FeS_2}, \quad (2)$$

where $\Delta\mu_S$ and $\Delta\mu_{Fe}$ are the deviations of chemical potentials of S and Fe relative to their elemental phases (S_8 and bulk Fe), respectively. The calculated formation enthalpy of pyrite, $\Delta\mu_{FeS_2}$, is -1.19 eV per FeS_2 unit. Figure 2 gives results of ΔH_f as a function $\Delta\mu_S$ in a range -0.6 eV $< \Delta\mu_S < 0.0$ eV. Arrows in Fig. 2 mark positions of two typical experimental conditions that use H_2S and S_8 as the reservoirs of sulfur.

At the onset, we may exclude S-divacancy and interstitial sulfur, since $\Delta H_f(V_{S\text{-}S})$ is larger than 4 eV, and $\Delta H_f(S_i)$ is even higher (>8 eV, not shown in Fig. 2). On the contrary, Fe or S single vacancy may have appreciable concentration in pyrite samples. $\Delta H_f(V_{Fe})$ is only 1.75 eV if S_8 is the sulfur reservoir, and the lowest value of $\Delta H_f(V_S)$ is 2.36 eV under S-poor conditions (or, equivalently, Fe-rich conditions). Interestingly, the formation of the $V_{Fe\text{-}S}$ pair might be as easy as V_{Fe} or V_S, by removing either a S atom around V_{Fe} with an energy cost of 1.2 eV or an Fe atom around V_S with an energy cost of 0.12 eV in the S-rich condition. Therefore, we suppose that V_{Fe}, V_S, and $V_{Fe\text{-}S}$ are the main native defects in pyrite under equilibrium growth/annealing conditions.

Yu *et al.*[19] and Sun *et al.*[47] recently obtained comparable formation energies of 3.5 eV and 3.0 eV for V_S in the S_8 environment, and they argued that equilibrium densities of all native defects should be insignificant for samples prepared

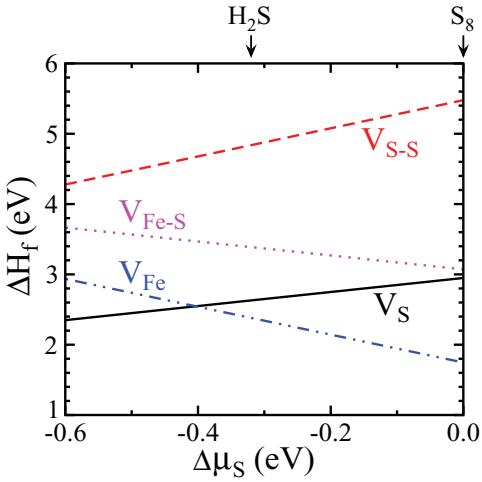

FIG. 2. (Color online) Formation energies of native defects, including V_S, $V_{S\text{-}S}$, V_{Fe}, and $V_{Fe\text{-}S}$ as a function of sulfur chemical potential ($\Delta\mu_S = \mu_S - \mu_S^0$, where μ_S^0 is the sulfur chemical potential of its elemental phase, S_8). The left and right boundaries of sulfur chemical potential correspond to the so-called Fe-rich (Fe bulk as the reservoir) and S-rich (S_8 as the reservoir) conditions, respectively.

at <800 K (<10^{11} cm^{-3}). However, one should accept these conclusions with caution. First, DFT studies of other materials suggest that defect formation energies are prone to overestimation. For example, the existence and importance of oxygen vacancies in metal oxides is well recognized despite very high calculated formation energies, e.g., ~3.0 eV for a bridging oxygen defect on rutile TiO_2(110) and ~4.0–5.3 eV for an oxygen vacancy in bulk rutile and anatase TiO_2.[60] Second, pyrite thin films may be prepared using non-equilibrium conditions with nonstoichiometric supplies of iron and sulfur. Large deviations in FeS_2 stoichiometry (>1 at.%) have been reported in many studies using elemental analysis, x-ray diffraction, and density measurements,[22,24] but these findings were blamed on measurement error and sample contamination in the review by Hopfner and coworkers, who concluded that there is no definitive proof whether or not pyrite is nonstoichiometric.[61,62] In their view, pyrite is probably a line compound with a sulfur-to-iron ratio of 2.00 (i.e., a phase width of less than 1%). A number of papers have found substantial nonstoichiometry in polycrystalline pyrite thin films using Rutherford backscattering spectrometry (which has a best-case accuracy of ~1 at.%), energy dispersive spectroscopy, and similar techniques.[61,63–66] However, the presence of sulfur-deficient phase impurities (in cases of S:Fe < 2.00) or excess sulfur at surfaces and grain boundaries (in cases of S:Fe > 2.00) may explain most if not all of these results. Evidence for sulfur divacancies and vacancy clusters in pyrite by positron annihilation spectroscopy has also been reported,[16] but these studies are in our view preliminary and far from conclusive. We conclude that the longstanding question of pyrite stoichiometry remains unsettled. Of course, even if pyrite is stoichiometric at the percent level, native defects that may be present at parts per billion to parts per thousand could be sufficient to dope pyrite films and dominate their electronic properties.

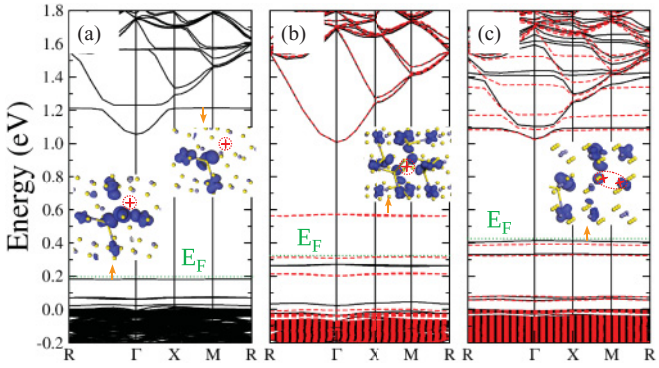

FIG. 3. (Color online) Band structures of a $3 \times 3 \times 3$ pyrite supercell with (a) V_S, (b) V_{Fe}, or (c) $V_{Fe\text{-}S}$. The black solid and red dashed lines in (b) and (c) represent majority- and minority-spin bands, respectively. The VBM is set as the reference energy for each case. The horizontal green dotted lines indicate the corresponding Fermi level of each case. The insets provide the isosurfaces of single state charge densities (at 0.03 e/Å^3) of the defect states, indicated by arrows. Violet (dark) and yellow (light) spheres represent Fe and S atoms, respectively. The cross signs in dotted circles denote the positions of the missing S or Fe atoms.

We now examine the impact of neutral V_S, V_{Fe}, and $V_{Fe\text{-}S}$ on the electronic properties of pyrite. It remains debatable whether S vacancies produce gap states in bulk pyrite, ever since Birkholz *et al.* reported that pyrite samples are sulfur deficient up to 12 at.%.[12] Although V_S has received significant attention in the literature, few studies have focused on V_{Fe} and $V_{Fe\text{-}S}$. From Fig. 3, it can be seen that all three types of vacancies produce defect levels in the band gap and near the band edges. Although the concentration of vacancies in our calculations is quite high (2.3×10^{20} cm^{-3}), the defect states are nearly dispersionless and thus their effect is well contained in the $3 \times 3 \times 3$ supercell. The presence of V_S induces two defect states in the band gap near the valence band and a resonant state within the conduction band, 0.08 eV, 0.18 eV, and 1.21 eV relative to the VBM. From the single-state charge-density plot in the left inset in Fig. 3(a), the gap state at 0.18 eV has mostly S-p_z and Fe-t_{2g} features around the S atom nearest to V_S and its three Fe neighbors. This state splits off from the valence band because cleavage of the S-S dimer changes the charge distribution around the sulfur vacancy. The state at 1.21 eV distributes around the S and three Fe neighbors of V_S, mostly with the S-p_z and Fe-e_g characters, as shown in the right inset of Fig. 3(a). The Bader charge state of the remaining S atom near V_S becomes $-0.75e$, almost double that of the S atom in the perfect bulk pyrite. The Bader charge states of the other atoms, including the neighboring Fe atoms of V_S, remain essentially unchanged. Therefore, the creation of V_S converts the remaining S atom in the dimer to S^{-2}.

Interestingly, V_{Fe} triggers spin polarization, with a sizeable magnetic moment of 2.0 μ_B/cell. The distribution of spin moment is rather delocalized, with 0.06 μ_B on each S atom around V_{Fe} and 0.15 μ_B on each second-nearest-neighbor Fe atom. The large spatial range of the spin polarization around V_{Fe} suggests potential long-range magnetic ordering in Fe-deficient pyrite, but more studies are necessary to confirm this possibility. The single-state charge density plot in the inset of Fig. 3(b) shows that the lowest unoccupied gap state in the minority spin channel (0.57 eV above the VBM) consists of the p_z orbitals of the six sulfur atoms around V_{Fe} and the t_{2g} orbitals of the twelve Fe atoms adjacent to them. The pronounced doubly degenerate gap state in the majority-spin channel 0.27 eV above the VBM has a similar character but is occupied. There are two other gap states in the minority-spin channel, approximately 0.21 eV and 0.31 eV above the VBM, and their counterparts in the majority-spin channel are in the VB, manifesting the large exchange splitting for Fe-t_{2g} states. It appears that neutral V_{Fe} is neither a good donor nor a good acceptor since the impurity levels are far from both VB and CB.

Similarly, $V_{Fe\text{-}S}$ also induces a spin moment of 2.0 μ_B/cell, with the spin density distribution in close analogy to that of V_{Fe}. The band structure in Fig. 3(c) shows several defect states in the gap, along with a few resonant states in CB. In particular, two pairs of defect levels locate near the Fermi level: 0.33 eV and 0.40 eV above VBM in the majority-spin channel and 0.32 eV and 0.39 eV above VBM in the minority-spin channel. The single-state charge density in the inset in Fig. 3(c) for the defect state near E_F indicates it is mainly from Fe-3d orbitals. The defect levels of $V_{Fe\text{-}S}$ in the band gap are all occupied, so that neutral $V_{Fe\text{-}S}$ defects are deep donors in pyrite.

For the convenience of comparison, we extract the main defect levels of different vacancies from their band structures and plot them on top of the band gap of perfect pyrite in Fig. 4. Sulfur vacancies create states within the band gap, as originally proposed in the qualitative ligand field theory model of Birkholz *et al.*[12] and developed by Bronold *et al.*[13,15] The latter authors argue that V_S forms easily with a concentration of 10^{20}–10^{21} cm^{-3} and creates mid-gap states that induce large thermionic-field emission currents in the dark, leading to the low V_{OC} of pyrite electrochemical and Schottky junctions.[62] However, our calculations show that bulk V_S creates gap states quite close to the VBM and hence is probably not responsible

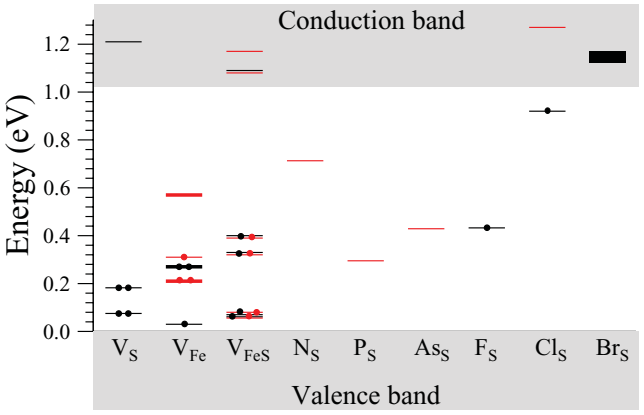

FIG. 4. (Color online) Kohn-Sham defect levels for a $3 \times 3 \times 3$ supercell containing one vacancy or impurity with respect to the valence and conduction bands (shaded regions) of the perfect bulk pyrite. Black and red (dark gray) lines denote defect levels in the majority and minority spin channels, respectively. Thick lines for V_{Fe} denote double degeneracy of defect states, and the rectangle for Br_S indicates a Br-induced resonant band. Dots represent the electron occupancy of the neutral defects.

TABLE II. Binding energies (E_b, in eV), induced spin moments (M_S, in μ_B), bond lengths ($d_{I\text{-}S}$, in Å), and Bader charge states of the impurity-S dimers (Q_I and Q_S for impurity and S atoms, respectively, in electron charge) for various substitutional dopants in pyrite.

Impurity	S_S	O_S	N_S	P_S	As_S	F_S	Cl_S	Br_S
E_b	−2.95	−3.11	−0.60	−2.49	−1.75	−3.56	−1.73	−0.97
M_S	0.00	0.00	1.00	1.00	1.00	1.00	1.00	0.81
d_{I-S}	2.16	1.73	1.74	2.15	2.26	2.59	2.56	2.56
Q_I	−0.43	−1.65	−1.07	+0.59	+0.68	−0.75	−0.51	−0.29
Q_S	−0.43	+0.62	−0.13	−1.37	−1.27	−0.55	−0.55	−0.55

for the low V_{OC} of pyrite Schottky solar cells. Mechanisms that greatly increase the concentration of V_S, V_{Fe}, or $V_{Fe\text{-}S}$ (e.g., non-equilibrium conditions, or lower defect formation energies near the crystal surface) would make the causal connection between vacancies and low V_{OC} as advocated by Bronold *et al.* more plausible. Theoretical studies of surface and near-surface defects in pyrite are ongoing and will be reported elsewhere.[67] Of course, the electronic behavior of a defect state also depends on its charge state or by the Fermi energy of the system. For example, while neutral sulfur vacancies are very deep donors, positively charged sulfur vacancies are likely to act as shallow acceptors according to the energy diagram in Fig. 4. Similarly, neutral V_{Fe} is a deep trap/recombination center for carriers, whereas negatively charged V_{Fe} is a deep donor. Self-consistent calculations for different charge states are needed to explore the effect of local charge on impurity levels, as were done for several defected systems.[68–70]

C. The effect of substitutional oxygen (O_S) impurities

Oxygen may be incorporated in pyrite samples during growth and annealing processes, and thus it is important to investigate the electronic properties of O-doped pyrite. The ionic radius of oxygen is slightly smaller than that of sulfur, and oxygen has a much larger electronegativity (3.44 for O vs 2.58 for S). Sun *et al.* recently argued that substitutional oxygen impurities can account for the *p*-type doping that is nearly always observed for nominally undoped pyrite thin films.[70] However, the validity of some assumptions in their model and analysis, including the experimental growth conditions needed to induce high oxygen concentrations, are questionable. For example, many pyrite thin films that have been reported to be *p*-type by thermopower measurements were fabricated in sulfur-rich, low-oxygen conditions rather than the iron-rich, oxidizing conditions emphasized by Sun *et al.*[70] These considerations motivated us to undertake a comprehensive analysis of the electronic effects of substitutional oxygen (O_S) in pyrite.

When one S is replaced by O in the $2 \times 2 \times 2$ supercell ($FeS_{1.97}O_{0.03}$), the O-S dimer binds more tightly than the S-S dimer. The S-O bond length of 1.73 Å in O-doped pyrite is significantly smaller than the S-S bond length (2.16 Å) in bulk pyrite. The Fe-O bond length, 2.32 Å, is nevertheless slightly larger than the Fe-S bond length in bulk pyrite (2.27 Å). To describe the strength of interaction for oxygen and other substitutional anion impurities in pyrite (discussed later), we define a binding energy:

$$E_b = E(I_S) - E(V_S) - \mu_I, \quad (3)$$

where $E(I_S)$ and $E(V_S)$ are the energies of pyrite with a substitutional impurity or V_S in the supercell, and μ_I is the chemical potential of the impurity atom. For simplicity, we set μ_I in their standard states, e.g., O_2 for oxygen, S_8 for S, and N_2 for nitrogen. Additional calculations are needed to determine μ_I if other impurity sources are used. The calculated values of E_b are given in Table II, where the result for S in a sulfur site (S_S, i.e., ideal pyrite) is listed for reference. One may easily show that E_b for S is equal to $-\Delta H_f(V_S)$ at S_8, as in Fig. 2. It is interesting that E_b of oxygen is slightly larger by 0.16 eV than that of sulfur. Although this value may change if alternative reservoirs of oxygen are used, it is clear that O_S binds more strongly than S_S in pyrite. Therefore, O_S can be effective to heal V_S defects of pyrite.

The effect of O_S on the electronic properties of pyrite is revealed in the total and projected DOS and band structure plotted in Figs. 5(a) and 5(b). We find that O_S removes the gap states induced by V_S and $FeS_{2-x}O_x$ ($x = 0.03$ for a $2 \times 2 \times 2$ supercell with one O_S) appear to be an intrinsic semiconductor. This is unsurprising given the identical valences and overall chemical similarity of oxygen and sulfur. Although the S-O bond is shorter than the S-S bond, the DOS curves of Fe and S atoms are not much different from those of perfect bulk pyrite. The DOS curve of oxygen is also very similar to that of sulfur, except that its 2p band is narrower [Fig. 5(a)]. From the band structure in Fig. 5(b), we find that the band gap of the hypothetical $FeS_{1.97}O_{0.03}$ crystal is about 1.06 eV, slightly larger than that of pyrite itself. The VBM shifts from near the X-point to *near* the Γ-point, as displayed in the inset of Fig. 5(b), which means that $FeS_{1.97}O_{0.03}$ is also an indirect gap semiconductor. The effective electron and hole masses at the CBM and VBM are estimated to be $0.54m_e$ and $2.05m_e$, close to the values for perfect bulk pyrite. Interestingly, $FeS_{1.99}O_{0.01}$ (a $3 \times 3 \times 3$ supercell with one O_S) has similar features, which implies that the properties of $FeS_{2-x}O_x$ compounds are independent of oxygen concentration lower than 3%. Therefore, incorporating a few percent or less of O into pyrite samples may reduce the concentration of V_S and their accompanying gap states, thereby cleaning the gap and improving the carrier mobilities and lifetimes.

Bader charge analysis reveals that the O-S dimer is strongly polarized, with charge states of $-1.65e$ and $+0.62e$ on the O and S sites, respectively. To more clearly depict the charge redistribution caused by O substitution, we calculated charge density difference, as shown in Fig. 5(c). It is obvious that the O atom gains electrons from its neighboring Fe and S atoms. In particular, the charge redistribution around the S atom in the O-S dimer is rather complex: the S atom gains electrons

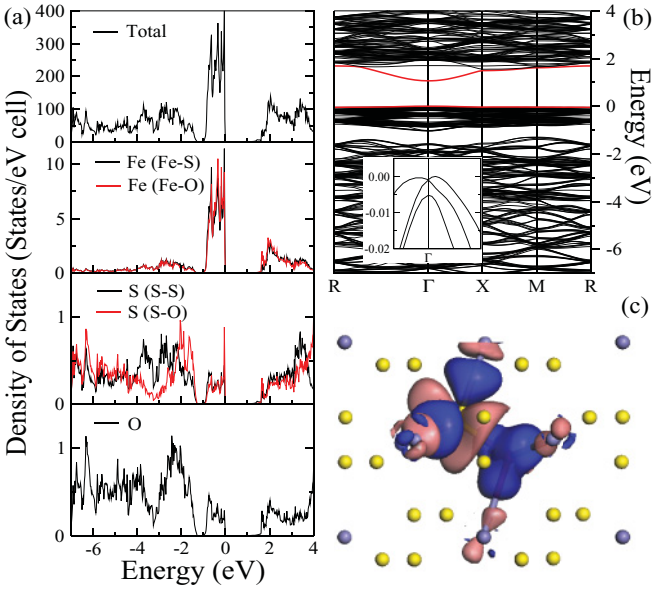

FIG. 5. (Color online) Results for oxygen-doped pyrite ($FeS_{1.97}O_{0.03}$). (a) Total and projected DOS. The notation in parentheses indicates the bonds to which the atoms belong. The VBM is set as the energy reference. (b) Band structure. The reference energy is the same as in (a). The red (dark gray) lines denote the topmost valence band and lowest conduction band. The inset is a magnified view of valence bands near the VBM around the Γ-point and the y-axis unit is eV. (c) Charge density difference [$\Delta\rho = \rho(O_S) - \rho(V_{S\text{-}S}) - \rho(O) - \rho(S)$] viewed in the (110) plane. Note that the atomic positions in reference systems were fixed as those in O-doped pyrite. The isosurfaces are at the values of $\pm 0.03\ e/\text{Å}^3$, with blue (dark) and red (light) regions for charge gain and loss, respectively. Violet (dark) and yellow (light) spheres represent Fe and S atoms, respectively.

from its three neighboring Fe atoms and donates electrons to the O atom. The O-S dimer with a Bader charge of $-1.03e$ is slightly more negative than the S-S dimers with a Bader charge of $-0.86e$. Accordingly, three Fe atoms near O_S have higher Bader charges ($+0.95e$) compared to other Fe atoms ($+0.86e$). Overall, the impact of O_S on the electronic properties of pyrite is rather local. We reiterate that the conventional viewpoint of inorganic chemistry—which labels ions only with integer charge states (e.g., Fe^{2+} and S^{1-})—is unrealistic because of the strong covalent nature of bonding in perfect and O-doped pyrite. Although a similar charge difference was found by Sun *et al.*,[70] it is improper to claim, as these authors did, that O_S is an acceptor based only on the assumed charge state of substitutional O (O^{2-}). The DOS and band structure in Fig. 5 clearly show no gap state induced by a neutral O_S.

D. Doping with Group V elements

To use pyrite in photovoltaic applications, it is crucial to control carrier concentrations and diffusion lengths through doping. Several groups have reported that substitution of phosphorus or arsenic for sulfur yields p-type conduction in pyrite, but the results for carrier concentration and mobility are rather scattered.[21–23] Here, we investigate the effects of N_S, P_S, and As_S impurities in order to understand the challenges involved in p-type doping with Group V elements. From Table II we can see that both N_S and As_S are energetically unfavorable because their binding energies are much smaller than S_S in bulk pyrite. In contrast, the binding energy of P_S is only 0.5 eV smaller than S_S, which implies that P has a reasonable probability to be incorporated into pyrite. This is expected based on the similar atomic sizes and electronegativity of P and S. Note that the values of E_b can be increased if less stable impurity sources are used. Therefore, N and As may still be doped in pyrite with more reactive impurity sources. We find that N_S, P_S, and As_S all make pyrite magnetic with a spin moment of 1.0 μ_B per impurity atom. The magnetic properties will be further discussed in detail.

Similar to the O-doping case, the N-S dimer has a very short bond (1.74 Å) when N replaces S atom in pyrite. The charge states of N and S are $-1.07e$ and $-0.13e$, respectively. This indicates that the N-S bond is also polarized due to the charge transfer from S to N. The charge state of Fe atoms near S remain nearly unchanged ($\sim+0.86e$), whereas Fe atoms near N_S lose more electrons to N and their Bader charge becomes $+0.98e$. Obviously, the N-S dimer attracts more electrons from Fe than does the S-S dimer. In the DOS plots in Fig. 6(a), one can see that nitrogen substitution produces several pronounced side peaks near the VBM, mainly from the Fe-t_{2g} states. In addition, it is clear that the DOS is spin-polarized, with a localized gap state at 0.7 eV above the VBM in the minority-spin channel (also see Fig. 4). As seen in the inset of Fig. 6(a), this gap state features mainly the t_{2g} orbitals of the six Fe atoms around the N-S dimer and the 2p orbitals of N and S.

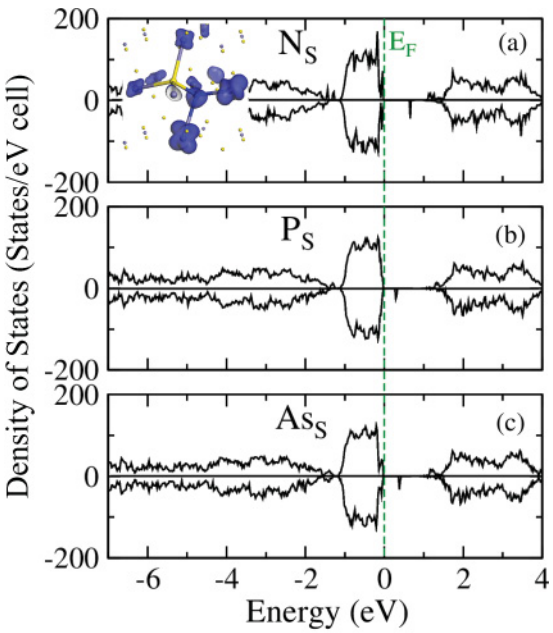

FIG. 6. (Color online) Total DOS of a $2 \times 2 \times 2$ pyrite supercell with a single (a) N_S, (b) P_S, and (c) As_S dopant, corresponding to a defect concentration of 7.8×10^{20} cm^{-3}. The vertical dashed line indicates the Femi energy. The positive and negative DOS indicate majority and minority spin channels, respectively. The inset in (a) shows the isosurfaces (at 0.01 $e/\text{Å}^3$) of the single-state charge density of the defect state induced by N_S in the minority spin channel at 0.7 eV above the VBM. Similar features were found for gap states of P_S and As_S.

Since N has one fewer valence electron than S, N_S is expected to be an acceptor in pyrite, but the acceptor level is about 0.7 eV above the VBM [Fig. 6(a)] and cannot ionize efficiently at room temperature. In this sense, neutral N_S centers are extremely inefficient dopants. N_S also reduces the local point group symmetry of the neighboring Fe atoms from O_h to C_{4v}; the t_{2g} states regroup to e-states (d_{xz} and d_{yz}) and b_2-state (d_{xy}) (here the z-axis is along the Fe-N bond).[71] As a result of charge redistribution and lattice distortion, the b_2 state becomes vacant in the minority-spin channel.

P_S and As_S are also deep acceptors in pyrite. As shown in Figs. 6(b) and 6(c), the DOS features are very similar to those of N_S, but their acceptor levels shift closer to the VBM (0.31 eV and 0.44 eV, respectively, as shown in Fig. 4). Therefore, heavily P- and As-doped pyrite is expected to be weakly p-type at 300 K via thermal excitation of electrons to these deep acceptor levels (ionization efficiency of 10^{-5}–10^{-8}). It is interesting that the carrier should be 100% spin-polarized since the acceptor level in the minority-spin channel only exchange electrons with states in VB with the same spin. This feature could be very useful for spintronics applications if the magnetic ordering is sustained at room temperature. Studies of magnetic properties of pyrite samples with large concentrations of P_S are desired to test these predictions.

Due to the very similar atomic sizes and electronegativities of P and S, the valence band is almost unaffected by P_S except that the b_2 state splits off. The bond length of the P-S dimer in P-doped pyrite is almost the same as that of S-S dimer (2.15 Å vs 2.16 Å), which indeed indicates minimal local structural change. Surprisingly, the charge states of P and S atoms are $+0.59e$ and $-1.37e$, respectively. This suggests a strong charge polarization in the vicinity of the P-S dimer, but in the opposite way compared to the O_S and N_S cases. The bond length of the As-S dimer in As-doped pyrite is 2.26 Å, and the charge states of the As and S atoms are $+0.68e$ and $-1.27e$, respectively. This sizeable structural distortion causes the upward shift of the As_S gap state compared to that of P_S.

Overall, the density of holes in N-, P-, and As-doped pyrite should be rather low near room temperature, with Boltzmann factors for thermal excitation ranging from 10^{-5} (for P_S) to 10^{-12} (for N_S). Other complex processes such as the formation of defect clusters and the activity of other impurities may easily produce larger carrier densities.[21,22] This may explain the scattered results of Hall measurements for p-type pyrite samples containing P and As.[21–23]

E. Doping with Group VII elements

Finally, we discuss the effect of the substitutional halogen impurities F_S, Cl_S, and Br_S in pyrite. Experimentally, substantial concentrations of halogen atoms may exist in pyrite crystals fabricated by chemical vapor transport (CVT) or chemical vapor deposition (CVD) when halogen transport agents (e.g., Br_2) or precursors (e.g., $FeCl_3$) are used. We find that F_S, Cl_S, and Br_S all lead to large structural distortions in pyrite, with S-F, S-Cl, and S-Br bond lengths of 2.59 Å, 2.56 Å, and 2.56 Å, respectively, about 18% longer than the S-S bond in bulk pyrite. Such a large bond length implies that the S-F, S-Cl, and S-Br dimers are actually broken. The binding energies listed in Table II indicate that F_S binds very strongly to its neighboring Fe atoms, with an energy gain of 0.61 eV per F atom relative to S_S. Therefore, F may easily replace S if F_2 gas is used as the impurity source and S_8 is the sulfur reservoir. The binding energy of Cl_S ($E_b = -1.73$ eV) is 1.22 eV smaller than S_S, meaning that substitution of each Cl for S costs 1.22 eV when Cl_2 is used as the source. The binding energy of Br_S is only -0.97 eV, so that substitution of Br for S costs 1.98 eV per atom. We emphasize again that the energies needed to form F_S, Cl_S, or Br_S (or indeed any impurity) depend strongly on both the impurity source and sulfur sink. For instance, taking the commonly used Cl source of $FeCl_3$ as reference, the binding energy is only -0.70 eV, which implies that the equilibrium Cl_S concentration should be very low when this source is used. Therefore, searching for chemically reactive doping sources is essential to achieve appreciable impurity concentrations in pyrite (as well as other semiconductors).

We now analyze the total and partial DOS plots of F_S- and Cl_S-containing pyrite in order to understand the electronic effects of halogen impurities. It can be seen from Figs. 7(a)–7(c) that F_S induces a state about 0.5 eV above the VBM in the majority-spin channel, which makes neutral F_S a deep donor in pyrite. Since the distance between F and S atoms is 2.59 Å, the F-S interaction is weakened whereas the p-d hybridization between F or S and their neighboring Fe atoms becomes stronger ($d_{\text{S-Fe}} = 2.27$ Å and $d_{\text{F-Fe}} = 2.22$ Å). This gives rise to a localized state in the band gap as well as resonant states in the valence and conduction bands, as shown in Figs. 7(a)–7(c). A net spin moment of 1.0 μ_B per atom is produced since F adds an extra electron to the system. Intriguingly, the spin polarization is rather delocalized, distributed mainly around the S atom adjacent to F ($M_S = 0.24\mu_B$) and the three Fe neighbors of S ($M_{Fe} = 0.27\ \mu_B$/Fe). The charge states of the F and S atoms are $-0.75e$ and $-0.55e$, respectively. This indicates that the $2p$ shell of the F atom is almost completely filled and the S atom near F also gains more electrons than other S atoms.

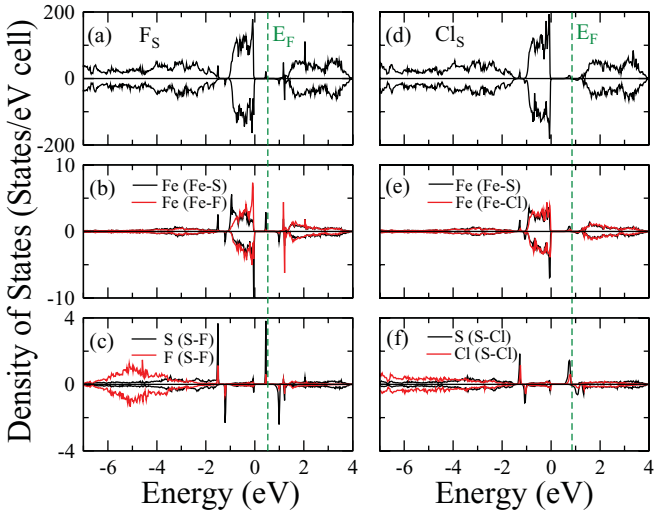

FIG. 7. (Color online) Total and projected DOS of a $2 \times 2 \times 2$ pyrite supercell with a single F_S (a)–(c) or Cl_S (d)–(f) defect. The respective VBM is set as the energy reference for both cases. The vertical dashed lines indicate the Femi energy. The positive and negative values of the DOS denote majority and minority spin channels, respectively.

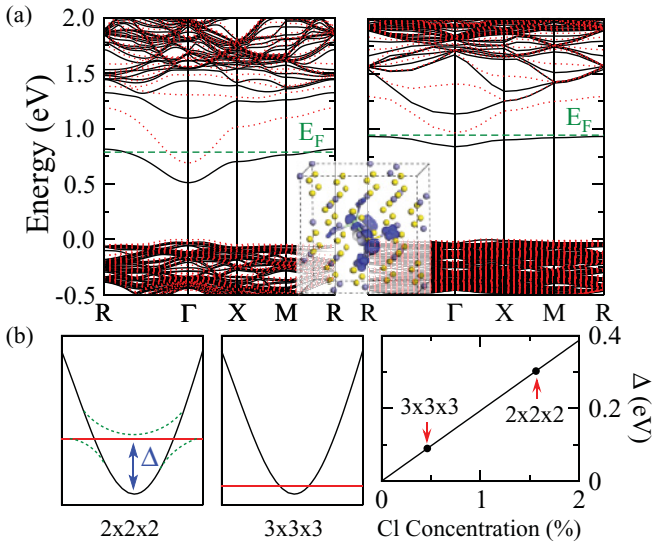

FIG. 8. (Color online) (a) Band structures of pyrite with a single Cl_S impurity in a $2 \times 2 \times 2$ supercell (left) and $3 \times 3 \times 3$ supercell (right). The solid black and dotted red (dark gray) lines denote the majority- and minority-spin states, respectively. The horizontal dashed lines give the Fermi energy for each case. The inset shows the spin density of $FeS_{1.97}Cl_{0.03}$, with the violet (dark) and yellow (light) spheres representing Fe, S, and Cl atoms, respectively. (b) Left and middle panels: sketches of the hybridization between the conduction band of pyrite (solid black line) and the atomic level of Cl (solid red/dark gray line) in $2 \times 2 \times 2$ and $3 \times 3 \times 3$ supercells, respectively. Right panel: the separation between Cl_S impurity level and CBM in the majority-spin channel as a function of Cl concentration.

Accordingly, the charge states of the Fe atoms adjacent to the F and S atoms are $+0.91e$ and $+0.98e$, respectively.

From Figs. 7(d)–7(f), we can see that Cl_S induces gap states near the CBM in both majority- and minority-spin channels. Due to the large size of Cl, the gap states are broad. From the band structure for the $2 \times 2 \times 2$ supercell in the left panel in Fig. 8(a), one can see a new dispersive band with an energy ranging from 0.5 eV to 0.8 eV in the majority-spin channel. Clearly, Cl-induced states strongly hybridize with the conduction states of pyrite, and thus one should actually view this system (one Cl_S in a $2 \times 2 \times 2$ supercell) as a chemical compound with a formula of $FeS_{1.97}Cl_{0.03}$. Furthermore, two Cl_S bands are partially occupied in both spin channels, and hence this heavily doped pyrite is metallic. Nevertheless, as displayed in the right panel in Fig. 8(a), the Cl_S band in the majority-spin channel becomes rather flat except in the vicinity of the Γ-point in the $3 \times 3 \times 3$ supercell ($FeS_{1.99}Cl_{0.01}$) that has a Cl_S density of 2.3×10^{20} cm^{-3}.

The formation of Cl_S bands can be simply understood by the hybridization of the atomic level of Cl and the conduction band of pyrite, as depicted in Fig. 8(b). This opens the conduction band of perfect pyrite and forms two new bands. The bandwidth of the lower new band, denoted as Δ, is the separation between Cl_S level and CBM. If we assume a linear dependence of Δ on the Cl_S concentration, we find that Δ approaches zero at the low Cl_S concentration limit. The position of the Cl_S level should be right under the CBM in typical samples that have Cl concentration of 10^{16}–10^{18}cm^{-3}. Cl_S impurities hence act as shallow donors and provide efficient n-type doping in pyrite.

Cl_S induces a magnetic moment of 0.996 μ_B and 1.000 μ_B in the $2 \times 2 \times 2$ and $3 \times 3 \times 3$ supercells, respectively. As displayed in the inset in Fig. 8(a), the spin density mainly distributes around the Cl-S dimer and its neighboring Fe atoms. The spin moments of Cl and S in the Cl-S dimer are 0.06 μ_B and 0.22 μ_B, respectively, while Fe atoms near the Cl or S atom possess 0.03 μ_B and 0.15 μ_B. Unlike F_S-containing pyrite, the charge states of Cl and S are $-0.51e$ and $-0.55e$, respectively. The charge states of Fe atoms ($+0.89e$) near Cl and S are not significantly different from perfect pyrite, even though Cl_S brings in an additional electron that is loosely bounded around the impurity.

The features of Br-doped pyrite (or more exactly the $FeS_{2-x}Br_x$ compound) are very similar to the Cl-doped case. Nevertheless, the mixed bands are somewhat broader due to the larger spatial extent of Br p-orbitals. The defect level of Br_S is hard to trace in $FeS_{1.97}Br_{0.03}$ but still shows as a broad resonance above CBM with a width of 0.12 eV in $FeS_{1.99}Br_{0.01}$, as depicted by a rectangle in Fig. 4. The reliable determination of Br level at low concentration hence needs calculations with $4 \times 4 \times 4$ or larger supercell, which are arduous even on parallel computers at this stage. We believe that the Br-doping level is close to CBM at low concentration and it should produce n-type pyrite, as does Cl.

IV. CONCLUSIONS

In summary, the properties of native point defects and substitutional anion impurities in iron pyrite were studied using spin-polarized DFT calculations. Our results indicate that the commonly held notion that sulfur vacancies are donors and iron vacancies are acceptors may be incorrect because these native defects, when neutral, induce localized and deep gap states that cannot easily contribute free carriers near room temperature. The large formation energies of these defects under typical experimental growth conditions imply very low equilibrium concentrations ($<10^{11}$ cm^{-3}) in the bulk, although surface defect concentrations may be substantially higher and are the subject of ongoing modeling and experimental studies in our labs. Our analysis shows that O_S centers are not electronic dopants in pyrite; in fact, gap states induced by sulfur vacancies can be eliminated by O_S impurities to produce a clean pyrite band gap. Based on our results, the ubiquitous observation of p-type conductivity in unintentionally doped pyrite thin films must be explained by factors other than bulk oxygen doping (e.g., surface and subsurface defects). We find that it is difficult to produce p-type pyrite by simple substitutional doping with Group V elements (N, P, and As) because the defect states lie near the middle of the band gap. However, the Group VII impurities Cl_S and Br_S are shallow donors that should efficiently produce n-type pyrite. All of the anion impurities induce a localized spin moment, making doped pyrite a possible ferromagnetic semiconductor for spintronics applications. Further studies of different charge states are necessary for more complete understanding of the effects of vacancies and dopants on the photovoltaic properties of pyrite.

ACKNOWLEDGMENTS

We thank the NSF SOLAR Program (Award CHE-1035218) and the UCI School of Physical Sciences Center for Solar Energy for support of this work. Calculations were performed on parallel computers at NERSC and at NSF supercomputer centers.

*wur@uci.edu

[1] R. Asahi, T. Morikawa, T. Ohwaki, K. Aoki, and Y. Taga, Science **293**, 269 (2001).
[2] W. Zhu, X. Qiu, V. Iancu, X. Q. Chen, H. Pan, W. Wang, N. M. Dimitrijevic, T. Rajh, H. M. Meyer, M. P. Paranthaman, G. M. Stocks, H. H. Weitering, B. Gu, G. Eres, and Z. Zhang, Phys. Rev. Lett. **103**, 226401 (2009).
[3] A. Schlegel and P. Wachter, J. Phys. C: Solid State Phys. **9**, 3363 (1976).
[4] P. P. Altermatt, T. Kiesewetter, K. Ellmer, and H. Tributsch, Sol. Energy Mater. Sol. Cells **71**, 181 (2002).
[5] A. Ennaoui and H. Tributsch, Sol. Energy Mater. **14**, 461 (1986).
[6] G. Smestad, A. Ennaoui, S. Fiechter, H. Tributsch, W. K. Hofmann, M. Birkholz, and W. Kautek, Sol. Energy Mater. Sol. Cells **20**, 149 (1990).
[7] C. Wadia, A. P. Alivisatos, and D. M. Kammen, Environ. Sci. Technol. **43**, 2072 (2009).
[8] A. Ennaoui, S. Fiechter, Ch. Pettenkofer, N. Alonso-Vante, K. Büker, M. Bronold, Ch. Höpfner, and H. Tributsch, Sol. Energy Mater. Sol. Cells **29**, 289 (1993).
[9] A. Ennaoui, S. Fiechter, W. Jaegermann, and H. Tributsch, J. Electrochem. Soc. **133**, 97 (1986).
[10] K. Buker, N. Alonso-Vante, and H. Tributsch, J. Appl. Phys. **72**, 5721 (1992).
[11] N. Alonso-Vante, G. Chatzitheodorou, S. Fiechter, N. Mgoduka, I. Poulios, and H. Tributsch, Sol. Energy Mater. **18**, 9 (1988).
[12] M. Birkholz, S. Fiechter, A. Hartmann, and H. Tributsch, Phys. Rev. B **43**, 11926 (1991).
[13] M. Bronold, C. Pettenkofer, and W. Jaegermann, J. Appl. Phys. **76**, 5800 (1994).
[14] K. Ellmer and H. Tributsch, in *Proceedings of the 12th Workshop on Quantum Solar Energy Conversion—(QUANTSOL 2000)* (Wolkenstein, Südtirol, Italy, 2000).
[15] M. Bronold, Y. Tomm, and W. Jaegermann, Surf. Sci. Lett. **314**, L931 (1994).
[16] S. M. Sze and K. K. Ng, *Physics of Semiconductor Devices* (Wiley, New Jersey, 2007).
[17] R. Murphy and D. R. Strongin, Surf. Sci. Rep. **64**, 1 (2009).
[18] K. M. Rosso, U. Becker, and M. F. Hochella Jr., Am. Mineral. **84**, 1535 (1999).
[19] L. P. Yu, S. Lany, R. Kykyneshi, V. Jieratum, R. Ravichandran, B. Pelatt, E. Altschul, H. A. S. Platt, J. F. Wager, D. A. Keszler, and A. Zunger, Adv. Energy Mater. **1**, 748 (2011).
[20] S. Fiechter, J. Mai, A. Ennaoui, and W. Szacki, J. Cryst. Growth **78**, 438 (1986).
[21] G. Willeke, O. Blenk, Ch. Kloc, and E. Bucher, J. Alloys Compd. **178**, 181 (1992).
[22] O. Blenk, E. Bucher, and G. Willeke, Appl. Phys. Lett. **62**, 2093 (1993).
[23] I. J. Ferrer, C. DelasHeras, and C. Sanchez, Appl. Surf. Sci. **70-71**, 588 (1993).
[24] I. J. Ferrer, F. Caballero, C. De las Heras, and C. Sanchez, Solid State Commun. **89**, 349 (1994).
[25] Y. Tomm, R. Schieck, K. Ellmer, and S. Fiechter, J. Cryst. Growth **146**, 271 (1995).
[26] B. Thomas, K. Ellmer, W. Bohne, J. Röhrich, M. Kunst, and H. Tributsch, Solid State Commun. **111**, 235 (1999).
[27] S. W. Lehner, K. S. Savage, and J. C. Ayers, J. Cryst. Growth **286**, 306 (2006).
[28] H. Ohno, Science **281**, 951 (1998).
[29] I. Zutic, J. Fabian, and S. Das Sarma, Rev. Mod. Phys. **76**, 323 (2004).
[30] K. Sato, L. Bergqvist, J. Kudrnovský, P. H. Dederichs, O. Eriksson, I. Turek, B. Sanyal, G. Bouzerar, H. Katayama-Yoshida, V. A. Dinh, T. Fukushima, H. Kizaki, and R. Zeller, Rev. Mod. Phys. **82**, 1633 (2010).
[31] T. Dietl, Nat. Mater. **9**, 965 (2010).
[32] S. Guo, D. P. Young, R. T. Macaluso, D. A. Browne, N. L. Henderson, J. Y. Chan, L. L. Henry, and J. F. DiTusa, Phys. Rev. Lett. **100**, 017209 (2008).
[33] S. Guo, D. P. Young, R. T. Macaluso, D. A. Browne, N. L. Henderson, J. Y. Chan, L. L. Henry, and J. F. DiTusa, Phys. Rev. B **81**, 144424 (2010).
[34] T. Dietl, H. Ohno, F. Matsukura, J. Cibert, and D. Ferrand, Science **287**, 1019 (2000).
[35] G. Kresse and J. Furthmuller, Comput. Mater. Sci. **6**, 15 (1996).
[36] G. Kresse and J. Furthmuller, Phys. Rev. B **54**, 11169 (1996).
[37] J. P. Perdew, K. Burke, and M. Ernzerhof, Phys. Rev. Lett. **77**, 3865 (1996).
[38] P. E. Blöchl, Phys. Rev. B **50**, 17953 (1994).
[39] G. Kresse and D. Joubert, Phys. Rev. B **59**, 1758 (1999).
[40] P. Bayliss, Am. Mineral. **74**, 1168 (1989).
[41] H. J. Monkhorst and J. D. Pack, Phys. Rev. B **13**, 5188 (1976).
[42] I. Opahle, K. Koepernik, and H. Eschrig, Phys. Rev. B **60**, 14035 (1999).
[43] J. Muscat, A. Hung, S. Russo, and I. Yarovsky, Phys. Rev. B **65**, 054107 (2002).
[44] J. Paier, M. Marsman, K. Hummer, G. Kresse, I. C. Gerber, and J. G. Ángyán, J. Chem. Phys. **124**, 154709 (2006).
[45] A. Rohrbach, J. Hafner, and G. Kresse, J. Phys.: Condens. Matter **15**, 979 (2003).
[46] S. Miyahara and T. Teranishi, J. Appl. Phys. **39**, 896 (1968).
[47] R. Sun, M. K. Y. Chan, and G. Ceder, Phys. Rev. B **83**, 235311 (2011).
[48] V. N. Antonov, L. P. Germash, A. P. Shpak, and A. N. Yaresko, Phys. Status Solidi B **246**, 411 (2009).
[49] A. M. Karguppikar and A. G. Vedeshwar, Phys. Stat. Sol. (a) **95**, 717 (1986).
[50] N. Hamdadou, A. Khelil, and J. C. Bernède, Mater. Chem. Phys. **78**, 591 (2003).
[51] A. K. Abass, Z. A. Ahmed, and R. E. Tahir, J. Appl. Phys. **61**, 2339 (1987).

[52]A. M. Karguppikar and A. G. Vedeshwar, Phys. Status Solidi A **109**, 549 (1988).
[53]M. Y. Tsay, Y. S. Huang, and Y. F. Chen, J. Appl. Phys. **74**, 2786 (1993).
[54]W. W. Kou and M. S. Seehra, Phys. Rev. B **18**, 7062 (1978).
[55]T. R. Yang, J. T. Yu, J. K. Huang, S. H. Chen, M. Y. Tsay, and Y. S. Huang, J. Appl. Phys. **77**, 1710 (1995).
[56]M. S. Seehra and S. S. Seehra. Phys. Rev. B **19**, 6620 (1979).
[57]G. L. Zhao, J. Callaway, and M. Hayashibara, Phys. Rev. B **48**, 15781 (1993).
[58]J. Cai, I. Goliney, and M. R. Philpott, J. Phys. Condens. Matter **18**, 9151 (2006).
[59]W. Tang, E. Sanville, and G. Henkelman, J. Phys. Condens. Matter **21**, 084204 (2009).
[60]M. V. Ganduglia-Pirovano, A. Hofmann, and J. Sauer, Surf. Sci. Rep. **62**, 219 (2007).
[61]C. Hopfner, K. Ellmer, A. Ennaoui, C. Pettenkofer, S. Fiechter, and H. Tributsch, J. Cryst. Growth **151**, 325 (1995).
[62]K. Ellmer and C. Hopfner, Philo. Mag. A **75**, 1129 (1997).
[63]S. Fiechter, Solar Energy Mater. Solar Cells **83**, 459 (2004).
[64]B. Thomas, T. Cibik, C. Hopfner, K. Diesner, G. Ehlers, S. Fiechter, and K. Ellmer, J. Mater. Sci.-Mate. Electron. **9**, 61 (1998).
[65]G. Chatzitheodorou, S. Fiechter, R. Könenkamp, M. Kunst, W. Jaegermann, and H. Tributsch, Mater. Res. Bull. **21**, 1481 (1986).
[66]B. Meester, L. Reijnen, A. Goossens, and J. Schoonman, Chem. Vapor Depos. **6**, 121 (2000).
[67]Y. Zhang, J. Hu, M. Law, and R. Q. Wu (unpublished).
[68]A. S. Foster, F. Lopez Gejo, A. L. Shluger, and R. M. Nieminen, Phys. Rev. B **65**, 174117 (2002).
[69]G. Roma and Y. Limoge, Phys. Rev. B **70**, 174101 (2004).
[70]R. Sun, M. K. Y. Chan, S. Y. Kang, and G. Ceder, Phys. Rev. B **84**, 035212 (2011).
[71]A. Hung, J. Muscat, I. Yarovsky, and S. P. Russo, Surf. Sci. **513**, 511 (2002).